Adaptive optics multiphoton microscopy to study *ex vivo* ocular tissues

Juan M. Bueno
Emilio J. Gualda
Pablo Artal
Universidad de Murcia
Laboratorio de Óptica
Campus de Espinardo (CiOyN)
Murcia, 30100 Spain

Abstract. We develop an adaptive optics (AO) multiphoton microscope by incorporating a deformable mirror and a Hartmann-Shack wavefront sensor. The AO module operating in closed-loop is used to correct for the aberrations of the illumination laser beam. This increases the efficiency of the nonlinear processes in reducing tissue photodamage, improves contrast, and enhances lateral resolution in images of nonstained ocular tissues. In particular, the use of AO in the multiphoton microscope provides a better visualization of ocular structures, which are relevant in ophthalmology. This instrument might be useful to explore the possible connections between changes in ocular structures and the associated pathologies. © *2010 Society of Photo-Optical instrumentation Engineers*. [DOI: 10.1117/1.3505018]

Keywords: multiphoton microscopy; wavefront aberration; adaptive optics; human ocular tissue.

Paper 10192PRR received Jun. 8, 2010; revised manuscript received Aug. 27, 2010; accepted for publication Sep. 10, 2010; published online Dec. 20, 2010.

1 Introduction

Two-photon excitation fluorescence (TPEF) has become a valuable tool for high-resolution tissue imaging, since it was first demonstrated[1] in 1990. Similarly to TPEF microscopy imaging, second-harmonic generation (SHG) microscopy[2,3] was reported to be a technique of particular interest to study biological samples containing collagen.

Despite the intrinsic confocality and optical sectioning capabilities of these techniques, the resolution and contrast of TPEF and SHG microscopy images are limited by the wavefront aberrations (WAs) of the illuminating laser beam,[4,5] the microscope optics itself, and those of the specimen when imaging deeper into the sample.[6]

The correction of aberrations by means of adaptive optics (AO) was originally proposed for astronomy,[7] although it has been extensively used in other areas, notably in visual optics and ophthalmology.[8–12] The incorporation of a deformable mirror (DM) into a confocal (linear) microscope was successfully reported by Booth et al.[13] This approach and similar ones with a liquid crystal modulator have been used by different authors to improve nonlinear microscopy images using fluorescent beads[6,14,15] and biological samples such as muscle, pulmonary, brain, and intestine tissues,[15–18] skull bone,[19] fish larvae,[20] and mouse embryos,[18] among others.

However, in most of these previous experiments, the use of a wavefront sensor was avoided, optimizing the shape of the mirror through image-based algorithms to improve in-depth nonlinear microscopy imaging.[21] Similar techniques were also successfully tested in coherent anti-Stokes Raman scattering (CARS) microscopy images.[22]

We recently reported an improvement in TPEF imaging of *ex vivo* human retinal tissues by simple realigning of the laser system cavity, while beam WAs were controlled in an open loop.[5] In this paper, we present a step forward into the correction of the laser beam WAs with AO to improve the image quality in nonlinear microscopy of ocular tissues.

2 Methods

Figure 1 depicts the experimental layout. This combines a multiphoton microscope and the AO module. A femtosecond Ti:Sapphire laser (760 nm) was used for illumination. Before entering the microscope, the beam passes the AO module composed of a Hartmann-Shack (HS) wavefront sensor and a DM used, respectively, to measure and correct for the beam WAs. The HS sensor (WFS150-5C, Thorlabs Inc., Newton, New Jersey) sampled the wavefront with an array of microlenses (0.15-mm pitch and 3.7-mm focal length). The DM was a gold-coated microelectromechanical systems (MEMS)-type (Boston Micromachines, Cambridge, Massachusetts) with 140 actuators. The microscope was built on a modified inverted microscope (Nikon TE2000-U). A set of two nonresonant galvanometric mirrors (M1 and M2) scanned the sample in the XY plane. A long-working-distance objective was used [20×, numerical aperture (NA) = 0.5]. A *Z*-control motor moved the microscope objective to reach the plane of interest within the sample. The nonlinear backscattered signal emitted by the sample went back through the same objective and passed a dichroic mirror (DIM) and the corresponding spectral filter (F), to reach the detection unit (PMT and photon-counting unit). The filter placed in the detection channel enabled the registration of either TPEF (broadband fluorescence filter, 435 to 700 nm) or SHG (narrow-band spectral filter, 380 ± 10 nm) signals from the specimens under analysis. Image recording control and postprocessing were made via custom software. The average illumination power at the specimen plane was between 2 and 200 mW, depending on the sample. Nonlinear

Address all correspondence to: Juan M. Bueno, Universidad de Murcia, Laboratorio de Óptica, Campus de Espinardo, 30100, Murcia, Spain. Tel: 34-868888335; Fax: 34-868883528; E-mail: bueno@um.es.

1083-3668/2010/15(6)/066004/7/$25.00 © 2010 SPIE

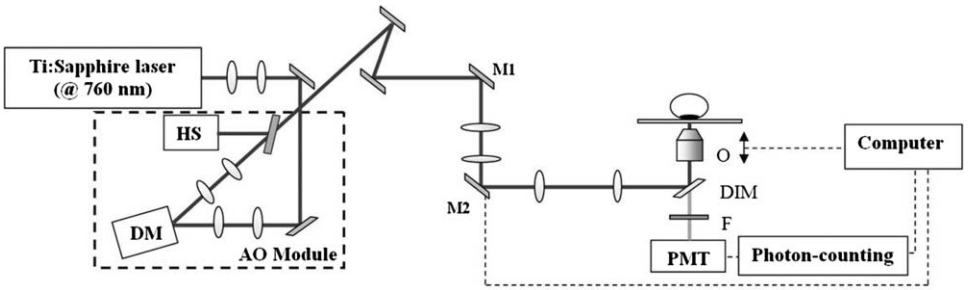

Fig. 1 Schematic of the AO multiphoton microscope: HS, Hartmann-Shack wavefront sensor; DM, deformable mirror; AO, adaptive optics module; M1 and M2, scanning mirrors; DIM, dichroic mirror; O, microscope objective; F, TPEF or SHG filter; PMT, photomultiplier.

microscopy images of different samples were registered with and without AO.

The laser beam WAs were estimated from the recorded HS images and expressed as a Zernike polynomial expansion up to fifth order across a 4-mm pupil, as explained elsewhere.[4,23] From each WA, the associated point spread function (PSF) was calculated. As image quality parameters, we used the root mean square (RMS) of the WA and the Strehl ratio. The appropriate DM shape to compensate for the measured WAs was determined in a closed loop.

Both nonbiological and biological samples were used in the experiments reported here. The former included a piece of paper stained with a fluorescent marker and a starch sample providing strong TPEF and SHG signals, respectively. As biological samples, we used both fresh and fixed nonstained human ocular tissues (retina, cornea, and sclera) and *ex vivo* porcine corneas.

Human tissues were extracted from ocular globes of healthy donors provided by the Ophthalmology Service of the Hospital Universitario Virgen de la Arrixaca, Murcia, Spain. Human corneas were excised with a trephine right after death. After trephination, the corneas were stored in Optisol and sent to the lab for analysis. After corneal removal, the rest of the ocular globes were immediately kept in a 0.9% sodium chloride solution and moved in an appropriate container from the hospital to the lab for the imaging of fresh *ex vivo* retinal tissues. Once there, the lens and the iris were carefully removed and the neurosensory retina excised. Both retinal tissues and corneas were placed in a glass-bottom dish surrounded by the same solution as that used for transportation, which ensured hydration during the whole experiment.

Thin (5-μm) fixed sections of human ocular tissue were embedded in paraffin as follows. Excised retinas and sclera portions were fixed with paraformaldehyde (4% solution in phosphate buffered saline) overnight to preserve the structure of the tissue. After a regular dehydration process using ethanol, this alcohol was cleared using xylene and the tissue was finally embedded in paraffin wax to become a solid block. This enabled a microtome to cut thin retinal sections of the specimen, which were mounted on a glass microscope slide.

Porcine ocular globes for corneal SHG imaging were obtained from a local slaughterhouse, kept in solution (see the preceding) immediately after death and moved to the lab. These intact eyes were placed upside down on a glass-bottom dish filled with solution during measurements. All corneas (human and porcine) appeared clear when viewed through a white-light microscope during the entire experiment and were neither fixed nor stained.

3 Results

In most optical systems, lower order aberrations (defocus and astigmatism) are the main contributors to the degradation of image quality. In microscopy, defocus does not affect the image quality since it can be corrected by refocusing the microscope objective. However, astigmatism is important since it produces two focal points and transforms these into ellipse-shaped spots. As an example, Fig. 2 shows the effect of astigmatism on the quality of nonlinear microscopy images of *ex vivo* human ocular tissues: the retinal nerve fiber layer (upper panels) and the corneal stroma (lower panels) providing TPEF[5] and SHG[24,25] signals, respectively. In both cases, the recorded signal levels in the images were noticeably reduced when astigmatism was present (28% in SHG and 73% in TPEF signals). For this particular test, a cylindrical lens was introduced in the light pathway. The HS measurement ensured that the use of this optical element did not introduce other significant (and unwanted) aberrations.

Figure 3 shows the laser beam WAs (up to fifth order) and their associated PSFs with and without AO. After aberration

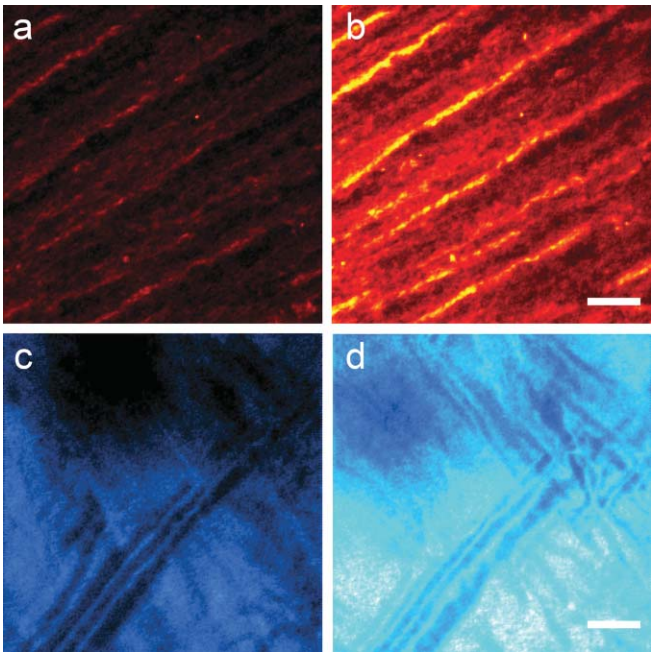

Fig. 2 Effect of inducing 0.5 diopters of astigmatism (panels on the left) on the image quality of nonlinear microscopy images of human ocular tissues: retinal nerve fibers imaged with TPEF signal, (a) and (b); and corneal stroma imaged with SHG signal, (c) and (d). Bar length: 35 microns. Pairs of images share the intensity scale.

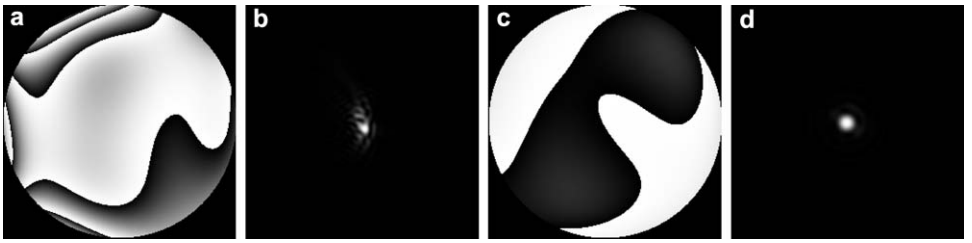

Fig. 3 Laser beam WA (2π-phasewrapped) (a) before and (c) after using AO correction. The associated PSFs, (b) and (d), subtend $\sim 1^{\circ}$.

correction, the RMS of the WA was reduced from 0.34 to 0.06 μm (Strehl ratio increased from 0.19 to 0.84). Figure 4 compares the corresponding individual Zernike coefficients (up to fourth order) of these WAs. Before correction (black bars), lower order aberrations [defocus (Z_0^2) and astigmatism terms (Z_2^{-2} and Z_2^2)] were the dominant contributors (75% of the total aberrations). After AO correction (white bars), the laser can be considered as nearly diffraction-limited.

As an evaluation of the effect of the laser beam WA correction on nonlinear microscopy, some images of nonbiological samples were acquired with and without AO. Figure 5 shows images of a stained piece of paper and a sample containing starch granules. An increase in the total signal intensity of around 50% for TPEF and 2.5-fold for SHG was reached. Moreover, additional spatial details are observed in the aberration-corrected images (see arrows on the image).

We also explored the image improvement in the nonlinear signal from fixed ocular tissues using beam WA correction. Figure 6 presents the TPEF and SHG images of nonstained transversal (*XZ*) thin sections of human ocular tissues embedded in paraffin (see Sec. 2). The upper panels show TPEF images of the retina and the lower panels contain SHG images from the sclera collagen.[26] The improvement in signal when the AO module was in operation can be observed, leading to a total intensity increase of almost threefold for TPEF images and twofold for SHG images. Additionally, in Fig. 6(a) structures such as the retinal nerve fiber layer (RNFL), the photoreceptor layer (PRL), as well as the different intermediate layers, are also better visualized due to the increase in image contrast.

Figure 7 depicts the intensity values, along the horizontal sections indicated in Fig. 6, for the images acquired with (dashed line) and without AO (solid line). The increase of contrast along a horizontal section when AO is activated can be observed for both, TPEF [Fig. 7(a)] and SHG [Fig. 7(b)] imaging modalities.

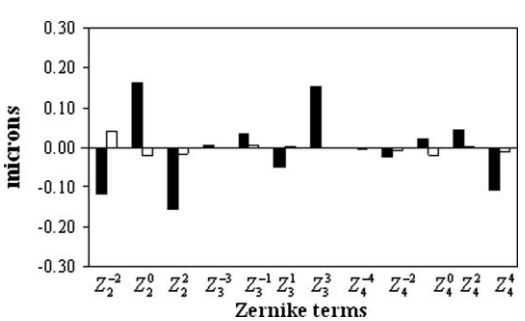

Fig. 4 Individual Zernike terms up to fourth order before (black bars) and after (white bars) using AO correction.

Nonfixed *ex vivo* ocular tissues were also analysed. As already reported, different corneal and retinal structures can be imaged under multiphoton microscopy without requiring fixation and/or staining procedures[5,27] due to endogenous fluorescence (autofluorescence) arising from specific fluorescent molecules or to the SHG signal originated from the corneal collagen within the stroma.[24,25] The benefit of using AO when imaging the *ex vivo* corneal stroma is presented in Fig. 8 for a plane located 150 μm below the corneal epithelium. An increase of 20% in the total intensity was found when using AO.

Finally, Fig. 9 compares the TPEF images of two different layers of an *ex vivo* human retina with and without AO: the area below the RNFL containing ganglion cells and blood vessels (BV) [Figs. 9(a) and 9(b)] and the photoreceptor layer [Figs. 9(c) and 9(d)]. In the upper panels, the total intensity in the images with AO was about three times higher than the case without AO, what provides a better visualization of the different retinal features. The enhancement of image containing

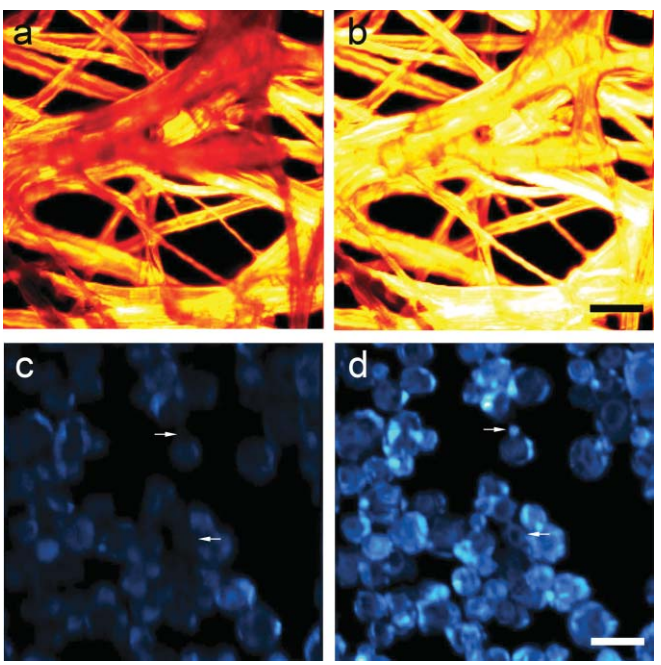

Fig. 5 (a) and (b) TPEF; and (c) and (d) SHG images of non-biological samples before, (a) and (c), and after, (b) and (d), laser beam aberration correction using AO. Samples correspond to a piece of fluorescent paper (a) and (b), and to a set of starch granules (c) and (d). Some features only observable when using AO are pointed with arrows. Each pair of images shares the intensity scale. Bar lengths: 70 (TPEF) and 16 (SHG) μm.

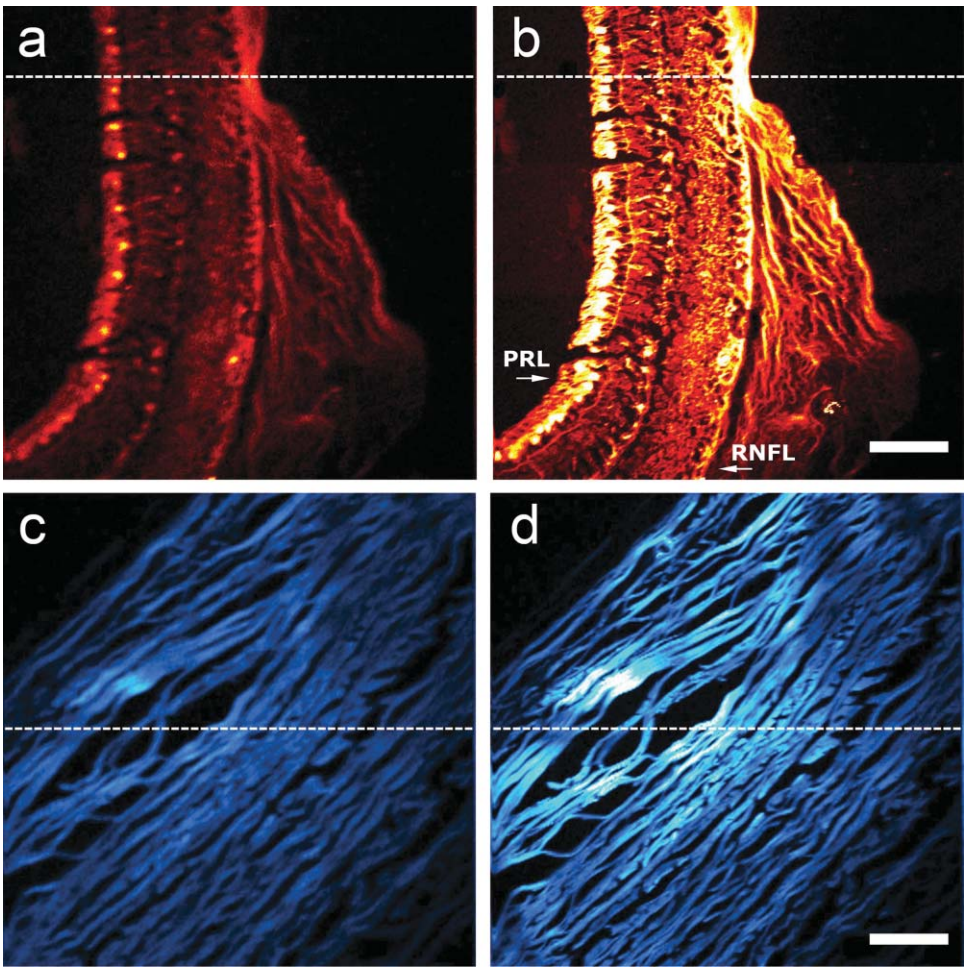

Fig. 6 Effects of using AO to compensate for the laser beam WAs on TPEF images of a histological section of a human retina (upper panels) and SHG images (lower panels) of a human sclera section with AO off (a) and (c), and AO on (b) and (d). The locations of the photoreceptor layer (PRL) and the retinal nerve fiber layer (RNFL) are indicated with arrows. Pairs of images share the same intensity scale. Bar length: 70 μm.

the human photoreceptor mosaic with AO in operation can be observed in Fig. 9(d).

4 Discussion

In the presented work, an AO multiphoton microscope is described. The AO module successfully corrects in closed loop for the aberrations of the ultrafast laser beam used as illumination source. With AO, a more compact PSF is obtained, potentially enhancing the intrinsic confocality and the contrast of nonlinear microscopy images.

Multiphoton microscopy has been extensively used for corneal imaging,[24,25] however, the analysis of retinal tissues has been mainly based on imaging the retinal pigment epithelium[27] (RPE) and the optic nerve head.[28,29] To our knowledge, this is the first time that AO multiphoton microscopy has been used

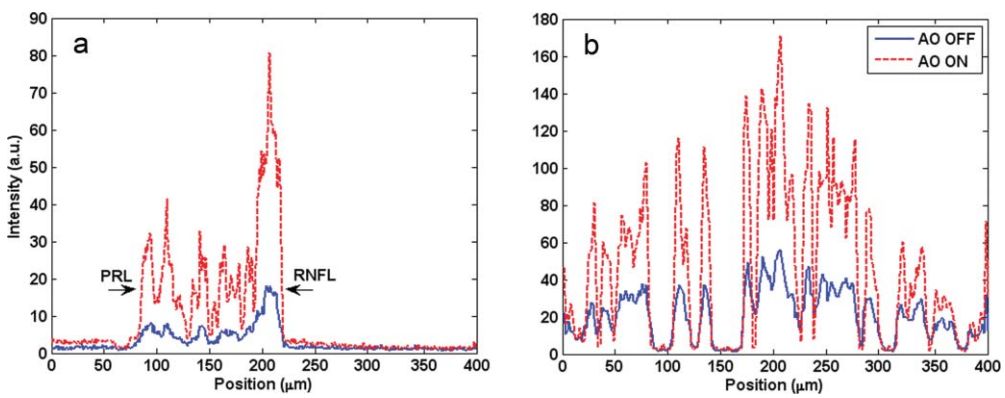

Fig. 7 Intensity values along the horizontal sections in Fig. 6 for the images acquired before (solid curve) and after (dashed curve) AO correction.

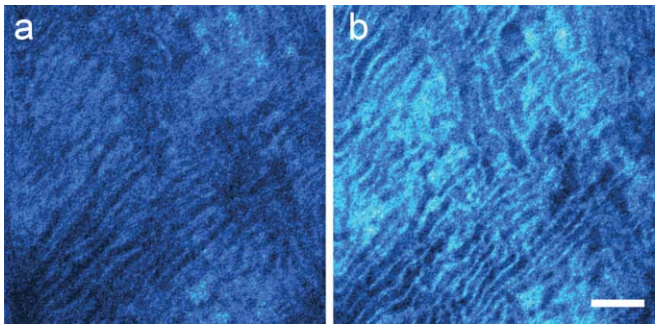

Fig. 8 (Color online) Effects of AO correction on SHG images of (neither fixed nor stained) porcine corneal stroma with (a) AO off and (b) AO on. The intensity scale was the same for both images. Bar length: 35 μm.

in image improvement of both fixed and nonfixed human ocular tissues. The instrument provides images with improved contrast and enhanced lateral resolution using a backscattered configuration.

Multiphoton imaging requires the use of ultrafast high-power lasers,[1,2] since these are unique sources able to produce nonlinear signals. However, these laser beams might be aberrated,[4] providing a first limit to nonlinear microscopy imaging. The use of AO devices to improve nonlinear microscopy images has been a topic of interest for the last decade. Neil et al. first reported a method to compensate for specimen-induced aberration correction by implementing a liquid crystal spatial light modulator into their nonlinear microscope.[14] The combination of a silver-coated membrane DM and a genetic algorithm was later demonstrated successfully.[6] Marsh et al.[15] also used a membrane DM (also without a WA sensor) to improve TPEF microscopy imaging. The procedure was based on the increase TPEF intensity levels within the image combined with other image-based merit functions.[21] The combination of an electrostatic deflected membrane mirror and a coherence-gated wavefront sensor also produced a significant improvement in two-photon microscopy images.[20] The approach used by Tsai et al. included a transparent deformable membrane with a vacuum behind to correct for spherical aberration,[16] and it was reported to improve axial resolution. Moreover, a sensor-less AO multiphoton microscope using a DM similar to the one presented in this paper was recently demonstrated.[18] Some of these previous papers used biological samples, such as muscles, tendons, brain tissue, larvae, or embryos among other.

Today, AO multiphoton microscopy is mainly oriented to correct for the in-depth aberrations of the specimen to improve the image quality for the different planes within the sample. The

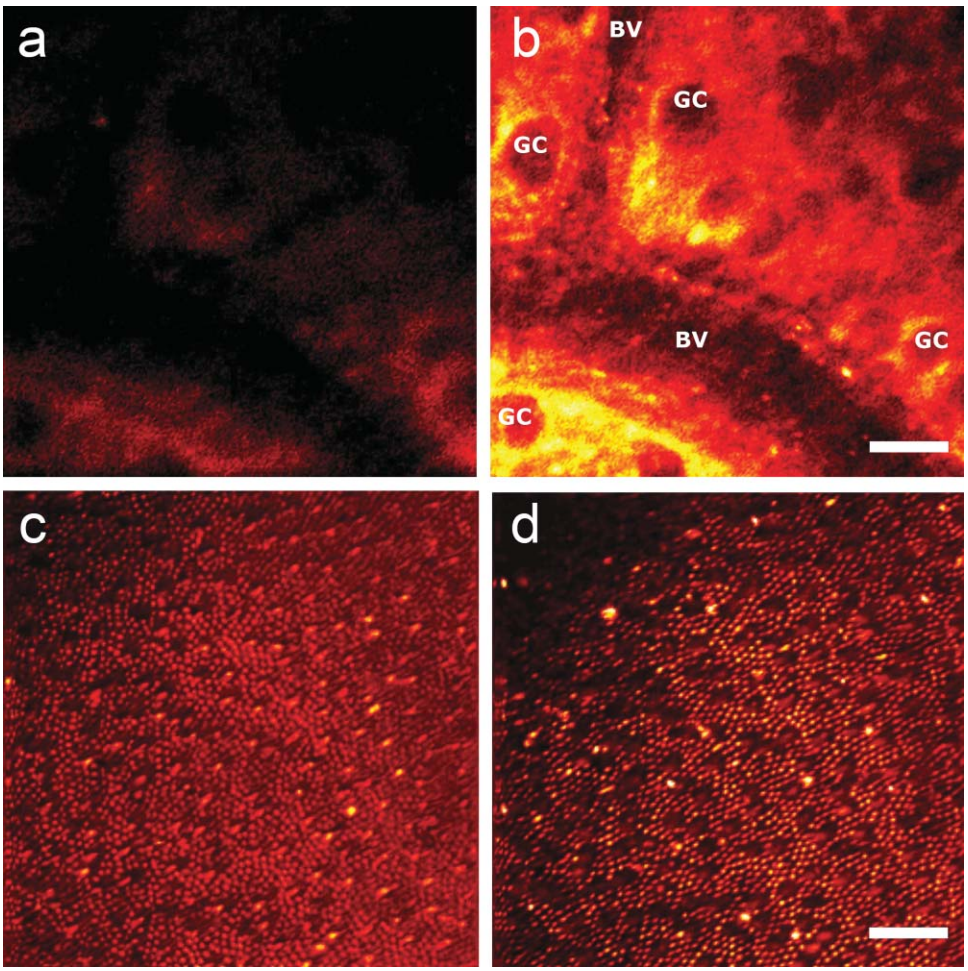

Fig. 9 TPEF images of a retinal area containing ganglion cells (GC) and blood vessels (BV) (upper row) and the photoreceptor layer (lower row) of an *ex vivo* human retina, (a) and (c) without and (b) and (d) with AO. Pairs of images share the intensity scale. Bar length: 35 μm.

DM shape was changed to optimize the image quality based on different metrics and some assumptions about the properties of the sample are often needed.[18] Despite the actual WA at a particular plane is not measured (i.e., sensorless technique), these experimental systems provide enhanced images of a number of biological samples.

Here, a different approach was used: the accurate measurement and compensation of the laser beam WAs (i.e., wavefront sensor plus DM). We report how the use of a DM to compensate just for the aberrations of the illumination beam can also improve ocular tissue imaging, meaning that a nonnegligible portion of the aberrations of the microscope are due to the illumination beam itself. This provides a useful tool to improve nonlinear microscopy imaging, without the requirement for complex and time-consuming genetic algorithms.

When the correction of the laser beam WAs is required, both the DM and the HS sensor must stand with the high power levels of the source. We recently reported a procedure to measure the WA of a high-power laser with a HS sensor.[4,5] Moreover, the gold coating of the DM makes it appropriate for this kind of experiment. For this particular implementation, the selected MEMS DM provides a stroke large enough to correct for the laser WAs. However, we must take into account that before AO operation, a realignment of the laser cavity was performed to improve the beam quality.[4,5] This operation represents a simple and effective solution for the partial correction of static low-order aberration correction (defocus and astigmatism), which might not be appropriately corrected by the DM if they present very high values, due to the mirror's limited stroke.

The impact of the laser beam WA correction on two-photon microscopy imaging was shown in ocular tissue imaging. For all samples, the use of AO caused an increase in both TPEF and SHG signals, which ranged between 20 and 200% for the cases here reported. This led to a better image quality, an improvement in contrast, and an enhancement of the lateral resolution. In particular, AO provided a better visualization of the complex layered retinal structure as well as some interlayer connections (see Fig. 7) in fixed samples.

Moreover, TPEF *XY* images of intact retinas (Fig. 9) were also noticeable improved when using AO. From a clinical point of view, two areas of interest have been imaged: the ganglion cells and the mosaic of photoreceptors. A better visualization of neither fixed nor stained human retinal structures will help in morphology studies as well as in the evaluation, follow-up, and understanding of some retinal pathologies (age-related macular degeneration, diabetic retinopathy, etc.).

Moreover, the instrument reported here also enabled the improvement of the SHG signal from biological tissues such as the sclera [Figs. 6(c) and 6(d)] and the corneal stroma (Fig. 8). Although both tissues are mainly composed of collagen, the distribution of collagen fibers is quite different. Unlike the cornea,[24,25,30–32] multiphoton microscopy studies of the sclera are scarce in the literature.[26,30] Since the sclera is opaque, SHG microscopy does not penetrate deep inside and a multiphoton diagnosis of scleral diseases might be limited. We showed that for thin or transparent samples, the use of AO produces an image improvement due to the efficient concentration of energy at the focal plane and the optimization of the nonlinear processes. Then, the use of AO solutions may lead to an increase of the penetration depth in sclera analysis, since the corrected illumination beam may potentially penetrate more within the sclera thickness leading to better-contrast images of deeper areas. Numerical simulations on how the aberrations affect the penetration depth depending on the distribution and type of collagen will be of interest for future works.

The increase in the nonlinear signal and the related image enhancement reported in this paper may also be interesting in segmentation algorithms that automatically detect the different retinal layers. These algorithms are often used in optical coherence tomography (OCT) imaging,[33,34] which is an interferometric imaging method providing high-resolution, cross-sectional imaging of biological tissues. In ophthalmology, OCT has enhanced opportunities for clinical diagnosis resolving individual retinal layers, enabling anterior chamber imaging,[35–38] and enabling 3-D volumetric imaging of ocular structures. The combination of AO with OCT was also reported to improve the contrast in retinal imaging when ocular aberrations were compensated.[39–41]

Unlike OCT, multiphoton microscopy is not yet a commercially available technique for clinical imaging of living eyes. However, when future *in vivo* implementations are possible, the combination of both techniques would be of special interest in vision research and clinical environments, mainly for high-resolution imaging of ocular tissues, diagnosis and disease progression among others.

Although our results are centered on improving individual layers within the sample, this method represents the first step to improve multiphoton 3-D imaging of ocular tissues. The dynamic operation (i.e., closed loop) of our AO device will be important to produce customized WA patterns in the illumination beam to independently improve the nonlinear imaging of particular planes within the retina or the cornea, which are of interest for clinical purposes. In particular, the induction of controlled amounts of spherical aberration in the laser beam increases the depth of focus within the sample, independently of the specimen-induced aberrations. This enables a more in-depth imaging what is essential in the analysis of ocular tissues.[42]

To conclude, we developed an AO multiphoton microscope to improve the nonlinear imaging of human ocular tissues. The AO implementation produced images with enhanced contrast and resolution without noticeable photodamage. This image improvement is of huge interest to better visualize retinal and corneal layers through volume rendering reconstructions. Although the effects of this technique on 3-D nonlinear imaging are beyond the scope of this paper, the benefits of AO might be extended over the whole ocular tissue volume by performing an appropriate customization of the laser beam WAs while varying the plane of focus. This represents the starting point to produce 3-D multiphoton microscopy images of ocular tissues with increased quality that might be useful in clinical environments.

Acknowledgments

This work has been supported by Ministerio de Educación y Ciencia, Spain (Grants FIS2007-64765 & Consolider SAUUL CSD2007-00033) and Fundación Séneca, Murcia, Spain (Grant No. 04524/GERM/06). The authors thank J. M. Marín, MD, PhD, from the Hospital Universitario Virgen de

la Arrixaca, Murcia, Spain, for providing the ocular tissue samples.

References

1. W. Denk, J. H. Strickler, and W. W. Webb, "Two-photon laser scanning fluorescence microscopy," *Science* **248**, 73–76 (1990).
2. S. Fine and W. P. Hansen, "Optical second harmonic generation in biological systems," *Appl. Opt*. **10**, 2350–2353 (1971).
3. B. F. Hochheimer, "Second harmonic light generation in the rabbit cornea," *Appl. Opt*. **21**, 1516–1518 (1982).
4. J. M. Bueno, B. Vohnsen, L. Roso, and P. Artal, "Temporal wavefront stability of an ultrafast high-power laser beam," *Appl. Opt.* **48**, 770–777 (2009).
5. E. J. Gualda, J. M. Bueno, and P. Artal, "Wavefront optimized nonlinear microscopy of ex-vivo human retinas," *J. Biom. Opt.* **15**, 026007 (2010).
6. L. Sherman, J. Y. Ye, O. Albert, and T. B. Norris, "Adaptive correction of depth-induced aberrations in multiphoton scanning microscopy using a deformable mirror," *J. Microsc.* **206**, 65–71 (2002).
7. R. K. Tyson, *Principles of Adaptive Optics*, 2nd ed., Academic, San Diego, CA (1997).
8. J. Liang, D. R. Williams, and D. T. Miller, "Supernormal vision and high resolution retinal imaging through adaptive optics," *J. Opt. Soc. Am. A* **14**, 2884–2892 (1997).
9. E. J. Fernández, I. Iglesias, and P. Artal, "Closed-loop adaptive optics in the human eye," *Opt. Lett.* **26**, 746–748 (2001).
10. A. Roorda, F. Romero-Borja, W. J. Donnelly III, H. Quenner, T. J. Hebert, and M. C. W. Campbell, "Adaptive optics scanning laser ophthalmoscopy," *Opt. Express* **10**, 405–412 (2002).
11. P. M. Prieto, E. J. Fernández, S. Manzanera, and P. Artal, "Adaptive optics with a programmable phase modulator: applications in the human eye," *Opt. Express* **12**, 4059–4071 (2004).
12. D. X. Hammer, R. D. Ferguson, C. E. Bigelow, N. V. Iftimia, T. E. Ustun, and S. A. Burns, "Adaptive optics scanning laser ophthalmoscope for stabilized retinal imaging," *Opt. Express* **14**, 3354–3367 (2006).
13. M. J. Booth, M. A. A. Neil, R. Juškaitis, and T. Wilson, "Adaptive aberration correction in a confocal microscope," *Proc. Natl. Acad. Sci. U.S.A.* **99**, 5788–5792 (2002).
14. M. A. Neil, R. Juskaitis, M. J. Booth, T. Wilson, T. Tanaka, and S. Kawata, "Adaptive aberration correction in a two-photon microscope," *J. Microsc.* **200**, 105–108 (2000).
15. P. N. Marsh, D. Burns, and J. M. Girkin, "Practical implementation of adaptive optics in multiphoton microscopy," *Opt. Express* **11**(10), 1123–1130 (2003).
16. P. S. Tsai, B. Migliori, K. Campbell, T. N. Kim, Z. Kam, A. Groisman, and D. Kleinfeld, "Spherical aberration correction in nonlinear microscopy and optical ablation using a transparent deformable membrane," *Appl. Phys. Lett.* **91**, 191102 (2007).
17. A. Leray and J. Mertz, "Rejection of two-photon fluorescence background in thick tissue by differential aberration imaging," *Opt. Express* **14**, 10565–10573 (2006).
18. D. Débarre, E. J. Botcherby, T. Watanabe, S. Srinivas, M. J. Booth, and T. Wilson, "Image-based adaptive optics for two-photon microscopy," *Opt. Lett.* **34**(16), 2495–2497 (2009).
19. Y. Zhou, T. Bifano, and C. Lin, "Adaptive optics two-photon fluorescence microscopy," *Proc. SPIE* **6467**, 646705 (2007).
20. M. Rueckel, J. A. Mack-Bucher, and W. Denk, "Adaptive wavefront correction in two-photon microscopy using coherence-gated wavefront sensing," *Proc. Natl. Acad. Sci. U.S.A.* **103**, 17137–17142 (2006).
21. A. J. Wright, D. Burns, B. A. Patterson, S. Poland, G. J. Valentine, and J. M. Girkin, "Exploration of the optimisation algorithms used in the implementation of adaptive optics in confocal and multiphoton microscopy," *Microsc. Res. Tech.* **67**, 36–44 (2005).
22. M. Girkin, S. Poland and A. J. Wright, "Adaptive optics for deeper imaging of biological samples," *Curr. Opin. Biotechnol.* **20**, 106–110 (2009).
23. P. M. Prieto, F. Vargas-Martín, S. Goelz, and P. Artal, "Analysis of the performance of the Hartmann-Shack sensor in the human eye," *J. Opt. Soc. Am. A* **17**, 1388–1398 (2000).
24. A. T. Yeh, N. Nassif, A. Zoumi, and B. J. Tromberg, "Selective corneal imaging using combined second-harmonic generation and two-photon excited fluorescence," *Opt. Lett.* **27**, 2082–2084 (2002).
25. N. Morishige, W. M. Petroll, T. Nishida, M. C. Kenney, and J. V. Jester, "Noninvasive corneal stromal collagen imaging using two-photon-generated second-harmonic signals," *J. Cataract. Refract. Surg.* **32**, 1784–1791 (2006).
26. M. Han, G. Giese, and J. F. Bille, "Second harmonic generation imaging of collagen fibrils in cornea and sclera," *Opt. Express.* **13**, 5791–5797 (2005).
27. O. La Schiazza and J. J. Bille, "High-speed two photon excited autofluorescence imaging of ex-vivo human retinal pigment epithelial cells toward age-related macular degeneration diagnostic," *J. Biomed. Opt.* **13**(6), 064008 (2008).
28. D. J. Brown, N. Morishige, A. Neekhra, D. S. Minckler, and J. V. Jester, "Application of second harmonic imaging microscopy to asses structural changes in optic nerve head structure *ex vivo*," *J. Biomed. Opt.* **12**, 024029 (2007).
29. M. Agopov, L. Lomb, O. La Schiazza, and J. F. Bille, "Second harmonic generation imaging of the pig lamina cribrosa using a scanning laser ophthalmoscope-based microscope," *Lasers Med. Sci.* **24**, 787–792 (2009).
30. S. W. Teng, H. Y. Tan, J. L. Peng, H. H. Lin, K. H. Kim, W. Lo, Y. Sun, W. C. Lin, S. J. Lin, S. H. Jee, P. T. C. So, and C. Y. Dong, "Multiphoton autofluorescence and second-harmonic generation imaging of the ex vivo porcine eye," *Invest. Ophthalmol. Vis. Sci*. **47**, 1216–1224 (2006).
31. N. Morishige, T. Nishida, and J. Jester, "Second harmonic generation for visualizing 3-dimensional structure of corneal collagen lamellae," *Cornea* **28**, S46–S53 (2009).
32. J. M. Bueno, E. J. Gualda, and P. Artal, "Analysis of corneal stroma organization with wavefront optimized nonlinear microscopy," *Cornea* (in press, 2010).
33. E. Götzinger, M. Pircher, W. Geitzenauer, C. Ahlers, B. Baumann, S. Michels, U. Schmidt-Erfurth, and C. K. Hitzenberger, "Retinal pigment epithelium segmentation by polarization sensitive optical coherence tomography," *Opt. Express* **16**, 16410–16422 (2008).
34. A. Mishra, A. Wong, K. Bizheva, and D. A. Clausi, "Intra-retinal layer segmentation in optical coherence tomography images," *Opt. Express* **17**, 23719–23728 (2009).
35. W. Drexler, U. Morgner, R. K. Ghanta, F. X. Kärtner, J. S. Schuman, and J. G. Fujimoto, "Ultrahigh-resolution ophthalmic optical coherence tomography," *Nature Med.* **7**, 502–507 (2001).
36. M. Wojtkowski, R. Leitgeb, A. Kowalczyk, T. Bajraszewski, and A. F. Fercher, "In vivo human retinal imaging by Fourier domain optical coherence tomography," *J. Biomed. Opt.* **7**, 457–463 (2002).
37. J. A. Goldsmith, Y. Li, M. R. Chalita, V. Westphal, C. A. Patil, A. M. Rollins, J. A. Izatt, and D. Huang, "Anterior chamber width measurement by high-speed optical coherence tomography," *Ophthalmology* **112**, 238–244 (2005).
38. W. Drexler and J. G. Fujimoto, "State-of-the-art retinal optical coherence tomography," *Prog. Retin. Eye Res.* **27**, 45–88 (2008).
39. Y. Zhang, J. T. Rha, R. S. Jonnal, and D. T. Miller, "Adaptive optics parallel spectral domain optical coherence tomography for imaging the living retina," *Opt. Express* **13**, 4792–4811 (2005).
40. R. J. Zawadzki, S. M. Jones, S. S. Olivier, M. T. Zhao, B. A. Bower, J. A. Izatt, S. Choi, S. Laut, and J. S. Werner, "Adaptive-optics optical coherence tomography for high-resolution and high-speed 3D retinal in vivo imaging," *Opt. Express* **13**, 8532–8546 (2005).
41. E. J. Fernández, B. Hermann, B. Považay, A. Unterhuber, H. Sattmann, B. Hofer, P. K. Ahnelt, and W. Drexler, "Ultrahigh resolution optical coherence tomography and pancorrection for cellular imaging of the living human retina," *Opt. Express* **16**, 11083–11094 (2008).
42. J. M. Bueno, E. J. Gualda, and P. Artal, "Effects of wavefront control on two-photon microscopy of ex-vivo ocular tissues," in *Focus on Microscopy Meeting 2010*, *Program and Abstract Book*, p. 123 (2010).